Study of Fan Noise Reduction for Automotive Radiator Cooling Fans

ATSUSHI SUZUKI*1
TETSUO TOMINAGA*2
TSUYOSHI EGUCHI*2
TOSHIFUMI KUDO*2
TOMOSHIGE TAKATA*2

In order to reduce automotive radiator cooling fan noise, it is necessary to reduce the system's blade passing frequency noise (BPF), a periodical noise unpleasant to the ear, in addition to an overall noise reduction. The authors have successfully developed and applied a BPF noise prediction technique, which consists of a computational fluid dynamics (CFD) and sound wave propagation analyses prior to trial. The accuracy of the BPF noise prediction was verified through an element test. Further, the geometrical parameters influencing the BPF noise have been optimized by applying quality engineering to evaluate the effect of noise reduction.

1. Introduction

With the remarkable reduction of noise inside and outside cars, there has been an increasing demand in recent years to reduce the noise of automotive radiator fans installed in the engine compartment to ensure a comfortable environment for the passengers. The BPF (blade passing frequency) noise is considered to be especially unpleasant to the ear and is easily affected by non-uniform flows inside the engine compartment, so that when the fan components are integrated into a compact module such as a condenser radiator fan module (CRFM), it is very important to predict and reduce the BPF noise. However, experimental studies of CRFMs installed in various vehicles are not always realistic due to the high lead-time and development costs.

This paper introduces the results of accuracy verification of a BPF noise prediction technique and presents a design example, including quality engineering optimization of BPF-noise-sensitive shroud configurations.

2. Features of CRFM

Figure 1 shows an outline of an automotive CRFM. The CRFM for this research has the fan and heat exchangers arranged in the space of 500 mm (width) x 400 mm (height) x 75 mm (depth). Compact as the module is, it has narrow spaces upstream and downstream. The heat exchanger (condenser) for the air conditioning system is located in the most upstream position, so that when fitted, flows coming into the condenser from the radiator grill and bumper have non-uniform velocity distributions. The condenser fins help to correct the flow direction and to equalize the exit flow velocities. After passing through the condenser, the airflow passes downstream into the radiator. Here, the flow interacts with the clearance flow coming from between the condenser and the radiator. Inside the radiator, as in the condenser, the flow direction is corrected to promote uniform flow velocity distributions. Therefore, the flow becomes comparatively uniform passing through the radiator. After leaving the radiator, the air stream is contracted by the shroud as it flows from the rectangular radiator surface to the annular fan opening before flowing into the fan with non-uniform velocity distributions in the direction of fan rotation. Inside the fan, the flow pressure is increased, and the cyclic outgoing flow then interacts with the motor support beam located downstream from the CRFM, and with the engine and other components located further downstream within the engine compartment.

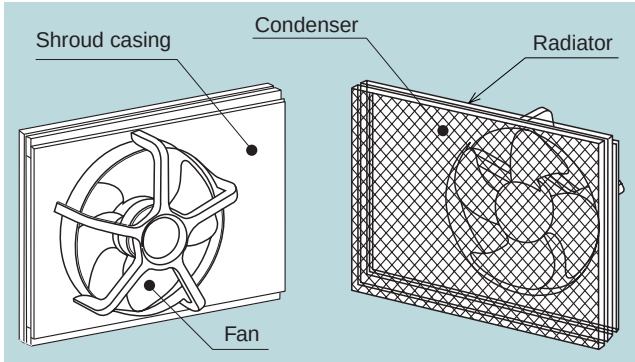

Fig. 1 Overview of automotive CRFM
Indicates the structural elements of the module.

3. Analogy of cause of BPF noise occurrence

The causes of BPF noise from a CRFM can be summarized as follows.

(1) Spatial transfer of pressure distributions generated on the blade surface by the fan rotation. (2) Time fluctuation of pressure distributions on the blade surface by non-uniform velocity distributions upstream of the fan. (3) Time fluctuation of pressure distributions on the blade surface by the potential interaction with engine components downstream of the fan. Thus, for BPF noise prediction, the use of a simulation method which can represent the three items above will be required.

*1 Air-Conditioning & Refrigeration Systems Headquarters
*2 Takasago Research & Development Center, Technical Headquarters

4. Modeling of CRFM

In order to facilitate a comparison between the predicted and experimental results for the BPF noise, a simplified model from the viewpoints of the flow and acoustic fields surrounding the fan was used. **Table 1** shows a list of the simplified models used for this research.

First, the circumferential non-uniformity is eliminated by removing the rectangular heat exchanger and the real shroud casing to allow a sufficiently large space composed only of a bellmouth casing with a circumferentially uniform cross-section and a cylindrical fan and motor support rod. Further, the non-uniform upstream velocity distributions are modeled by the wake generated by the obstacles (the flow interaction device) located upstream of the fan. On the other hand, the potential interactions are modeled by a flow interaction device located downstream of the fan. In order to investigate the degree of interaction of the upstream and downstream, flow interaction devices, straight type and cross type, were prepared.

5. BPF noise prediction method

In order to consider the change in the pressure field caused by the fan rotation and the cause of BPF occurrence, an unsteady CFD was carried out using sliding meshes to receive the fluctuations of the static pressure on the blade surface, the flow interaction device and the bellmouth casing as time series data. A universal thermal-liquid analysis code STAR-CD was used in this research. The calculation mesh used for the analysis, as shown in **Fig. 2**, consists of a total of 1200000 cells, with the bellmouth casing including the fan consisting of approximately 700000 cells. **Figure 3** shows the tested models and CFD mesh models, while **Table 2** shows the model dimensions and test conditions. In the unsteady calculation a 72-step frequency resolution per rotation was used, with the frequency resolution per time step being 3.3 kHz, approximately equivalent to 17 times the primary component of the BPF frequency (185 Hz). Thus, the frequency resolution is sufficiently high for BPF noise prediction. One cycle of rotation data of the static pressure values on all surface cells of one blade, the bellmouth casing and the flow interaction device for each time step were acquired. The authors have predicted the BPF noise of a CRFM based on simplified formula[1] by assuming the subsonic and far-distance acoustic fields, on the basis of Curle's formula[2], predicting a noise occurrence due to the pressure fluctuations on a solid wall surface.

$$p(\vec{x},t) = -\frac{1}{4\pi c}\int_s \frac{\sin\theta}{r}\left[\frac{\partial p_w(\vec{y})}{\partial t}\right] dS(\vec{y})$$

Table 1 Comparison of study models

	Shape of flow interaction device	Position of flow interaction device
Model 1	Straight-type	Inlet side
Model 2	Cross-type	Inlet side
Model 3	Straight-type	Outlet side
Model 4	Cross-type	Outlet side
Model 5	None	None

Table 2 Element test conditions

Items		Values
Fan diameter	(mm)	300
Number of blades		4
Rotating speed	(rpm)	2 770
BPF (primary)	(Hz)	185

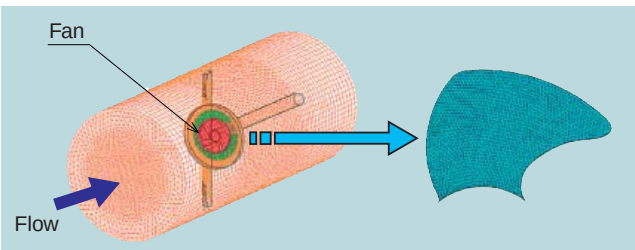

Fig. 2 Overview of experimental sample and Model 1

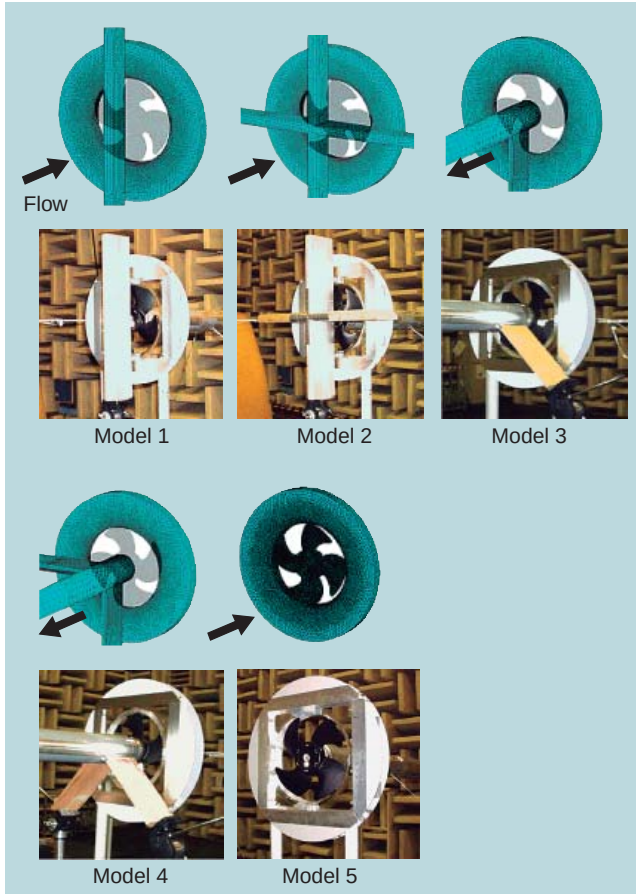

Fig. 3 Comparison between element test sample and experimental sample
Shows the comparison of models.

Where,

P (x,t): Sound pressure at observation point (Pa)

Pw (y): Pressure fluctuation at wall surface (sound source) (Pa)

dS: Area elements of each sound source (m^2)

c: Acoustic velocity (m/s)

r: Distance from sound source to observation point (m)

θ : Angle from sound source to observation point (rad)

[]: Delay on time (t-r/c)

The BPF noise was analyzed with an analysis code[3], which applied the above formula by regarding each wall surface cell as a sound source. In this analysis code, only the spatial distance decay between the sound source and the assessment point, the directivity concerning the time delay and the propagation, which are dependent on the sound velocity and the distance, are taken into consideration, with no consideration paid to reflection and diffraction. As shown in **Fig. 4**, the noise assessment points were positioned at regular intervals upstream of the shroud casing, where the influence of reflection and diffraction are negligible and the experimental difficulty is also reduced. The analysis code requires the calculation spatial grid coordinates of the unsteady calculation results, the coordinates of assessment points and the static pressure fluctuations on all the wall surfaces. As a result, the sound pressure time history and its FFT analysis results at the assessment points were obtained. The rotating system including the fan and the static system including shroud casing, etc. were individually analyzed, and the effect of sound pressure on the assessment points due to the surface wall static pressure was clarified.

6. Verification test of prediction accuracy

In order to carry out an experimental verification of the predicted results of the BPF noise, a test instrument equivalent to the analysis model was manufactured. **Figure 5** shows an overview of the test instrument. The noise was measured at the same measuring points as the assessment points shown in Fig. 4 with the test instrument. At each measuring point, the noise was measured with the noise measuring equipment with a 1/2 inch microphone made by Rion, and the frequency was also analyzed with a frequency analyzer. A maximum frequency of 2 kHz and frequency resolution of 1 Hz were obtained.

7. BPF noise prediction result

Figure 6 depicts the static pressure distribution on the solid surfaces around the fan obtained by the unsteady CFD analysis. As shown in the figure, atmospheric pressure can be observed on almost all the surfaces of the bellmouth and the flow interaction device while a high suction pressure can be observed on the fan blade surface. The analytical results, therefore, suggest that the static pressure fluctuation, which causes the BPF noise, can be considered to have a large amplitude on the rotor blade surface. The behavior of the temporal static pressure distribution was investigated focusing on the suction surface of the rotor blade where the influence of the flow interaction device is large. **Figure 7** shows the pressure distribution on the suction surface for Model 1. The vertical axis and color contour of the graph show static pressure on the blade as the relationship between the flow interaction device and the monitored rotor blade on the left side of the figure. As shown in the figure, the static pressure distribution on the rotor blade is the maximum on the blade leading edge, and is the minimum once it goes to the trailing edge and increases in a monotonic manner. Moreover, the minimum static pressure caused by the reverse flow from the rotor blade pressure surface exists in the tip section near the trailing edge.

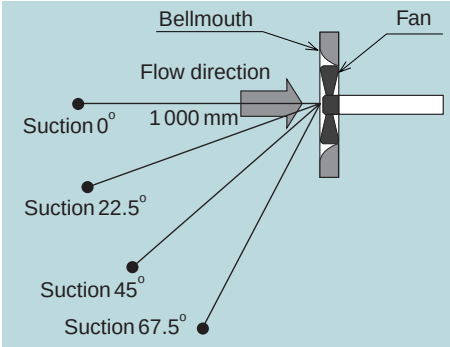

Fig. 4 BPF noise assessment points
Indicates the relation between the object of analysis and the noise assessment point.

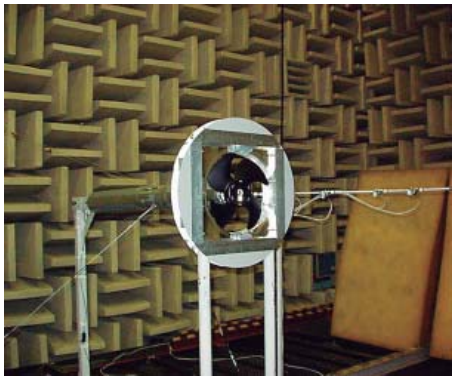

Fig. 5 Overview of test instrument
Indicates the state in the anechoic chamber.

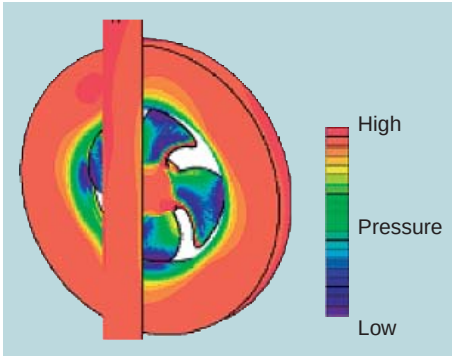

Fig. 6 Pressure distribution by flow analysis
Indicates the static pressure distribution throughout the fluid region.

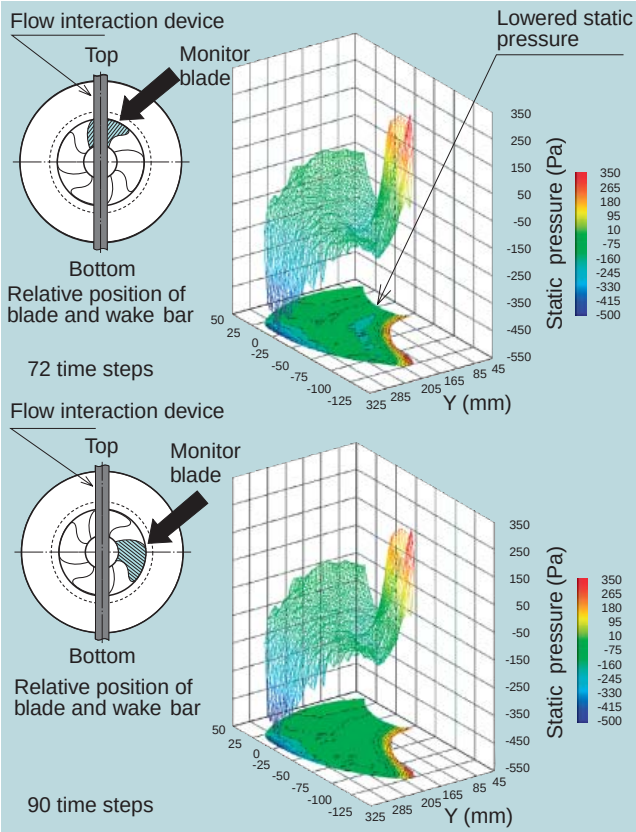

Fig. 7 Static pressure distribution on rotor blade
Indicates the instantaneous static pressure distribution of a rotating fan.

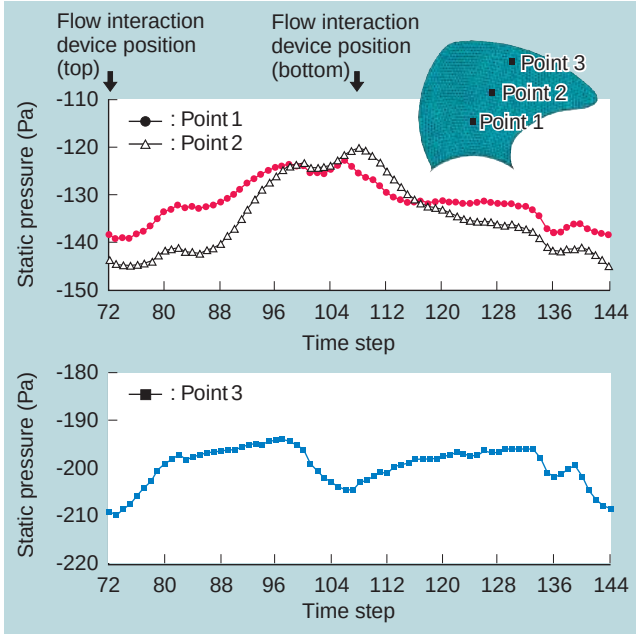

Fig. 8 Pressure change on fan blade surface
Indicates time record for one turn of fan.

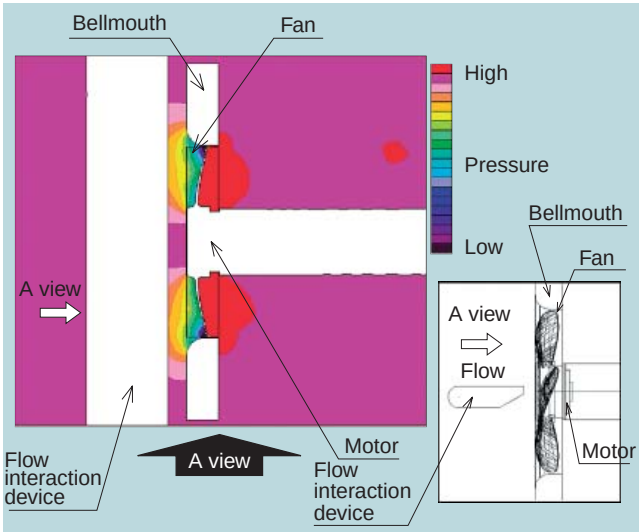

Fig. 9 Pressure distribution around flow interaction device and fan
Indicates the static pressure distribution in the center section of flow interaction device.

Turning attention to the change with time, the lower value can be observed around the mid-chord near the rotational center, compared with 90 time steps after a 1/4 turn in 72 time steps, which is attributed to the influence of the flow interaction device. The time history of static pressure values for a typical cell near the mid-chord was investigated as shown in **Fig. 8**. At Point 3 near the tip, wake interaction between the rotor blade and the flow interaction device can be observed, because the static pressure is found to be low in the vicinity of the flow interaction device. On the other hand, at Points 1 and 2 relatively near the rotational center, although the static pressure reduction due to wake interaction occurs near 72 time steps, the static pressure is increasing near 108 time steps. The amplitude of the static pressure fluctuation is about 15 Pa at Points 1 and 3, and the amplitude increases by 1.6 times to be about 25 Pa at mid-span Point 2. It is supposed that this phenomenon originates in the distance between the rotor blade and the flow interaction device and the non-axisymmetry of the flow interaction device. The static pressure distribution at the flow interaction device centerline cross-section is shown in **Fig. 9**. As the suction surface of the rotor blade approaches the rotational center from the blade tip, the distance from the flow interaction device becomes nearer, causing the static pressure value to increase. Moreover, in contrast with View A, the rotor blade which is above the fan center shaft in the contour figure, (i.e. near 72 time steps), approaches from a perpendicular side at the down side (108 time steps), to the rotor blade, approaching from the side where the flow interaction device is cut obliquely. For this reason, a phenomenon similar to the potential interaction occurs near the fan rotational center at 108 time steps, causing the static pressure to increase.

Next, the BPF components are extracted. These are considered to have great significance for BPF noise due to the static pressure fluctuation on the rotor blade surface. The magnitude of the static pressure BPF fluctuation component on the blade surface for Model 1 is shown in **Fig. 10**. The vertical axis of the graph and the color contours show the non-dimensional static pressure fluctuation which divides the rotor blade static pressure fluctuation by the bellmouth average inlet dynamic pressure.

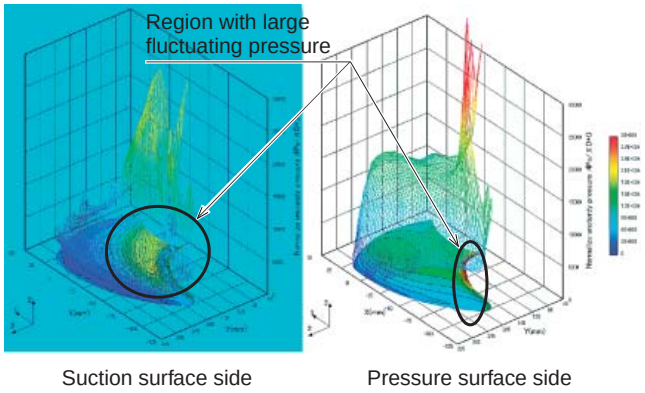

Fig. 10 Pressure fluctuation distribution on fan blade
Indicates amplitude of fluctuating pressure (non-dimensional value) on rotor blade pressure surface and suction surface of Model 1

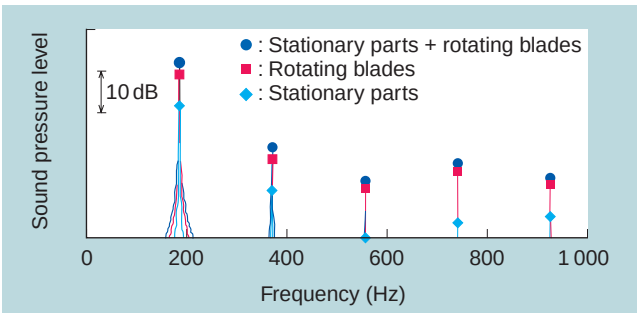

Fig. 12 Result of frequency analysis of sound waveform
Shows the large influence of the rotating blades.

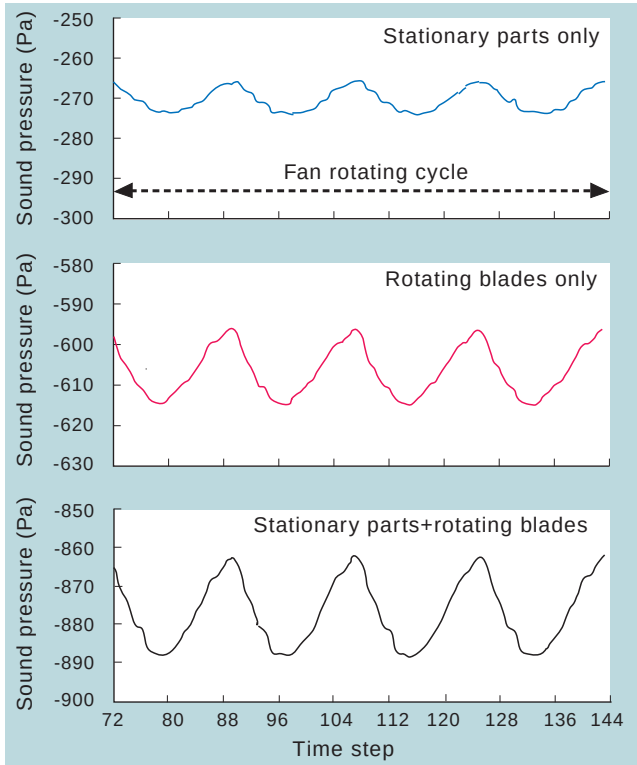

Fig. 11 Time history of sound pressure at assessment point (predicted)
Indicates the waveform per one turn of the fan at assessment point on suction side 0° of Model 1.

The high amplitude of the BPF component on the suction surface can be widely observed at the leading edge and at the mid-chord position near the rotational center of Model 1, in which the flow interaction device is installed upstream of the fan. This phenomenon is thought to occur due to the wake interaction near the tip, similar to the phenomenon of the occurrence of potential interaction near the rotational center. On the pressure surface, although a high fluctuation component exists in a few areas of the leading edge, the fluctuation becomes remarkably low in other areas because the influence of the flow interaction device is small.

Figure 11 shows the results predicted by the unsteady CFD and BPF noise analysis code, with the sound pressure waveform at the assessment point, suction 0 deg of Model 1. Each figure shows the predicted sound pressure wave results: the first obtained by the static system solid wall surfaces including the bellmouth casing and the flow interaction device; the second by the rotary system solid wall surfaces of 4 rotor blades; and the third by combining the first and second sound pressure waves. It turns out that each wave includes a four-cycle fluctuation, i.e. the BPF component. The sound pressure due to the effect of the stationary parts has an amplitude of about 8 Pa, while the sound pressure due to the effect of the rotating blades has about twice the amplitude, 15 Pa.

Figure 12 shows the sound spectra based on the frequency analysis with FFT. The spectra show the maximum peak value at the frequency of 185 Hz, which is the primary BPF component and also show clear peaks at the frequencies of the second (370 Hz) and the third (555 Hz) BPF components. In the higher level of components, except for the primary BPF, an extremely large difference of more than 20 dB in the sound pressure level can be observed. When comparing the first BPF spectra, a difference of 7 dB can be predicted between the peak levels due to the effect of the stationary parts and rotating blades. Moreover, the combined BPF noise level shows a large difference of 11 dB for the stationary parts, and the comparatively small difference of 3 dB for the rotating blades. As a result, the static pressure fluctuation on the solid surface in the rotating blades has a dominant influence on the peak level of BPF noise. It has been confirmed that this tendency is the same for all models except Model 1 and at all assessment points. **Figure 13** shows the predicted primary BPF noise level at each noise assessment point based on

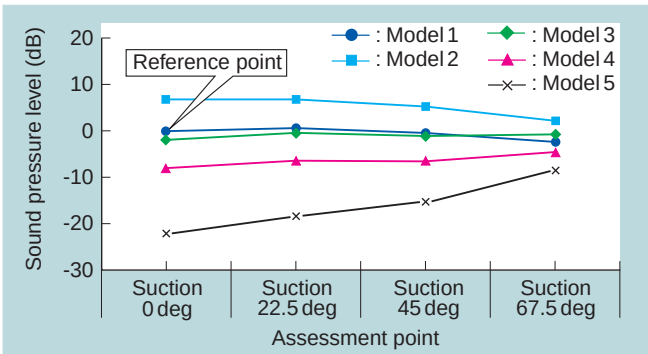

Fig. 13 Prediction result of BPF noise level (primary component)
Shows the prediction results at each assessment point for each model.

Model 1 as a reference. The value of the BPF noise has almost the same level at each noise assessment point, except for Model 5, without a flow interaction device. An especially remarkable directivity cannot be seen for Models 1 to 4 with flow interaction devices. On the other hand, for Model 5 with no flow interaction device, the smallest value is on the fan axis and it increases as it advances toward the fan radial assessment point. In Model 5, both the rotor blade and other stationary structure components are positioned in an axisymmetric manner, and if assuming that the flow field is completely axisymmetric, the noise of the BPF component will be generated only from the rotor blade load noise. For this reason, all the static pressure fluctuations from the solid wall surfaces are canceled at the assessment point on the fan axis and the sound pressure on the fan axis theoretically becomes zero. At radial assessment points, on the other hand, a BPF noise occurs due to the load noise resulting from the condition that the distance between the fan rotor blade and the assessment point is fluctuated by the fan rotation. The spatial distribution of the BPF noise predicted for Model 5 corresponds to the direction of propagation of the load noise. **Table 3** summarizes the BPF noise level for each model at each assessment point. This is equivalent to the energy generated by the sound source, i.e. the power level.

Model 2 > Model 1 > Model 4 > Model 3 > Model 5

Thus, the pressure fluctuation on the blade surface has the same relation for each model as described previously. It can, therefore, be deduced that the static pressure fluctuation on the blade surface is the main cause of BPF noise occurrence.

8. Experimental results of BPF noise

Figure 14 shows the results of noise measurement at the assessment point suction 0 deg for Model 1. As shown in the graph, the conspicuous peak values from the primary component (185 Hz) to the higher degree BPF components including the second (370 Hz) through the eighth (1,480 Hz) components can be observed. The primary BPF is highest at 66.8 dB and the level is 27 dB higher than the broadband noise level of about 40 dB. Similarly, the secondary BPF component with a level of 58.0 dB, the third component with a level of 62.2 dB and the fourth component with a level of 58.1 dB also have their peak values around 20 dB higher than the broadband noise level. Thus the BPF noise components are captured clearly by this experiment. For Models 1 to 5, the primary BPF component, which is shown in Fig. 14, has the highest value at all points of measurement, and the level is clearly higher than the broadband noise level.

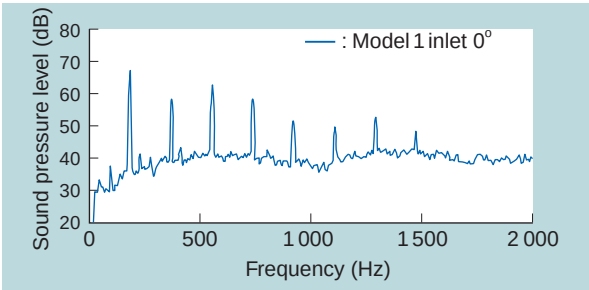

Fig. 14 Experimental sound spectrum at assessment point
Indicates sound pressure level at inlet side 0° assessment point of Model 1.

Table 3 Overall BPF noise level for each model (prediction)

	Shape of flow interaction device	Position of flow interaction device	BPF noise level
Model 1	Straight-type	Inlet side	0 dB
Model 2	Cross-type	Inlet side	6dB (relative to Model 1)
Model 3	Straight-type	Outlet side	−5.7 dB (ditto)
Model 4	Cross-type	Outlet side	−0.5 dB (ditto)
Model 5	None	None	−12.6 dB (ditto)

9. Comparison between predicted and experimental results

In order to verify the accuracy of BPF noise prediction, the BPF noise level obtained in this experiment was overlapped onto Fig. 13, the BPF noise prediction result, and plotted to compare the predicted value with the experimental value as shown in **Fig. 15**. The figure depicts the relative difference regarding the primary BPF noise level (185 Hz) for each assessment point for Model 1 and regarding the BPF noise level at the 0 deg assessment point of the suction side as the reference point, and the following items were confirmed through comparisons of the predicted and experimental values for Models 1 to 5.

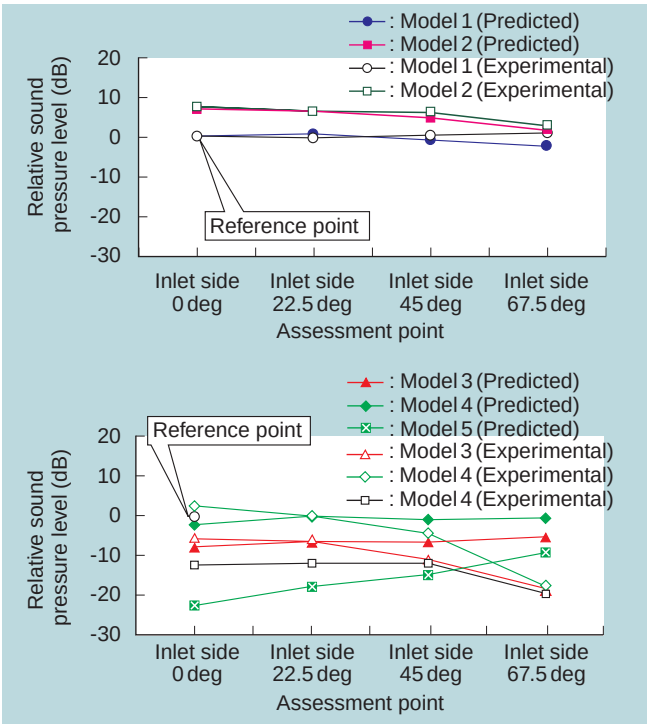

Fig. 15 Comparison between predicted and measured results
Indicates the results relative to BPF primary noise component (185 Hz).

(1) In the comparison of Models 1 and 2 with upstream flow interaction devices, the BPF noise level with "cross type" is about 7 dB higher than that with "straight type."
(2) In both cases with these flow interaction devices, no remarkable directivity can be seen.
(3) In the tendencies described above, both the experimental and predicted values are equivalent, and both relative differences show excellent agreement.
(4) In the comparison of Models 3 and 4 with downstream flow interaction devices, the experimental values differ from the predicted values. The BPF noise is predicted to be propagated throughout the suction side; on the other hand in the experiment it has directivity at a low level at the assessment points in the radial direction.
(5) Also, in Models 3 and 4, both relative differences coincide within the error of about 3 dB at the assessment points near the suction side in the axial direction (0 deg and 22.5 deg).
(6) In Model 5 with no flow interaction device, a big differences in the distribution and the level can be seen between the measured and the predicted values.

The difference between the predicted and experimental values for the cases where the flow interaction devices are installed downstream as described in (4) and (5), is attributed to the differences in the reflection of sound waves and the sound insulation not being taken into consideration in the prediction code. When a flow interaction device is installed upstream, since the static pressure fluctuation occurring on the rotor blade suction surface is the dominant factor for causing BPF noise, a solid wall surface which can shut off a sound wave at the noise assessment points does not exist. On the other hand, when the flow interaction device is installed downstream, the main static pressure fluctuation occurs on the rotor blade pressure side, and the rotor blade itself and the solid wall surface of the bellmouth casing, etc. exist in the noise assessment point area. For this reason, it is thought that the experimental values show relatively lower values at the assessment points in the fan radial direction than the predicted values.

In order to eliminate the influence of reflection, sound insulation, etc. as much as possible, the predicted value was compared with the experimental value with regard to the total sum of BPF noise levels at all assessment points with the first harmonic as a guideline corresponding to the power level. **Figure 16** shows the results thus obtained. In Models 1 to 4 with flow interaction devices, the figure shows excellent agreement, within 0.8 dB difference in the relative comparison between the predicted and the experimental values. As for Model 5 with no flow interaction device, there still exists a difference of about 2.5 dB. The reason for this is thought to be as follows. In the prediction, it is assumed that the flow from upstream

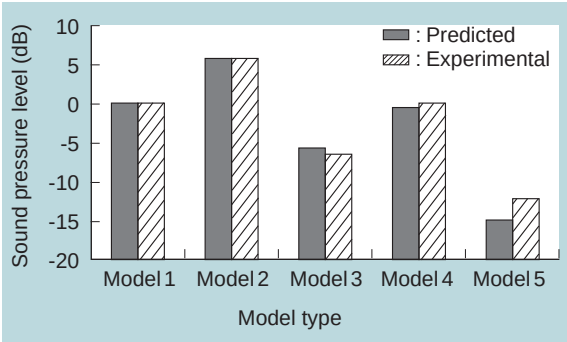

Fig. 16 Comparison of overall BPF noise level between predicted and measured result
Indicates high prediction accuracy for Models 1 to 4 with flow interaction devices.

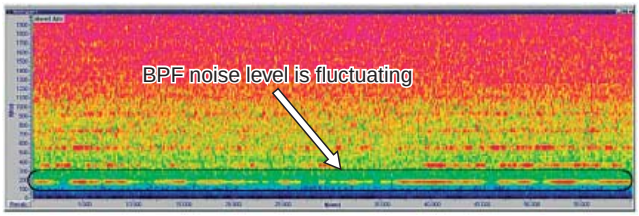

Fig. 17 Noise level in sonar graph
Indicates BPF noise level of Model 5 at assessment point of Inlet 0°.

is uniform and the code predicts periodic noise mainly due to load noise. In the measurement, on the other hand, the flow around the test instrument was not equalized sufficiently and it is thought that the BPF noise was amplified because the unstable periodic noise fluctuated at the low level and eventually occurred, as shown in **Fig.17**. However, in a CRFM, whose upstream and downstream flows do not become uniform in the direction of fan rotation, this tendency is not a problem. The results obtained from the present study, therefore, show that the BPF noise can be predicted with an accuracy of about 1 dB for the overall sound pressure, and within 3 dB for spatial distribution at the sound field where the effect of reflection and sound insulation is comparatively small. Hence, it has been confirmed that the newly developed technique has sufficient practical accuracy to predict the BPF noise of a CRFM.

10. Example of application of the BPF noise prediction method

In the CRFM design for each vehicle, a standard fan is used in order to reduce the lead time and development costs. Regarding the various problems (airflow rate, noise, input, etc.) to be considered when using a CRFM, it is generally acceptable to take countermeasures using the shroud casing which requires individual designs to be made for each vehicle. Moreover, since the shroud casing configuration and dimensions, etc. are comparatively sensitive to fan noise including BPF noise, it is mostly closed to the rotating blade. Therefore the authors carried out an optimization design for the shroud casing using the BPF noise prediction method in Fig. 1.

Table 4 Control and error factors for CRFM

Control factor		Level 1	Level 2	Level 3
A	Gap between strut and rotor blade (mm)	3	18	33
B	Width of strut (mm)	5	10	15
C	Fan diameter (mm)	300	277.5	255
D	Strut shape	Rectangle	Ellipse	Airfoil
Error factor		Level 1	Level 2	Level 3
A	External static pressure (Pa)	0	30	60

Table 5 $L_9(3_4)$ Orthogonal array for CRFM

Case	Control factor			
	A	B	C	D
1	Level 1	Level 1	Level 1	Level 1
2	Level 1	Level 2	Level 2	Level 2
3	Level 1	Level 3	Level 3	Level 3
4	Level 2	Level 1	Level 2	Level 3
5	Level 2	Level 2	Level 3	Level 1
6	Level 2	Level 3	Level 1	Level 2
7	Level 3	Level 1	Level 3	Level 2
8	Level 3	Level 2	Level 1	Level 3
9	Level 3	Level 3	Level 2	Level 1

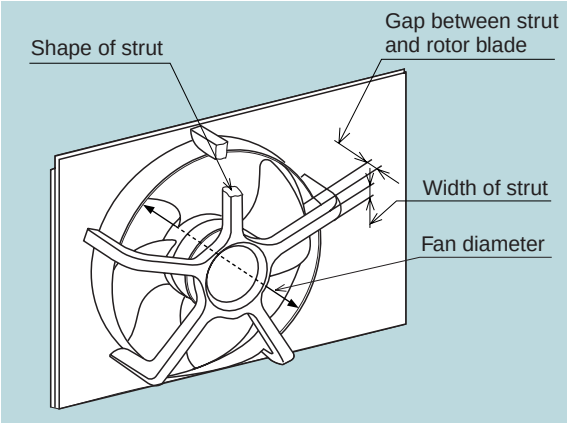

Fig. 18 Control factor for CRFM
Indicates the section extracted at the time of application of quality engineering.

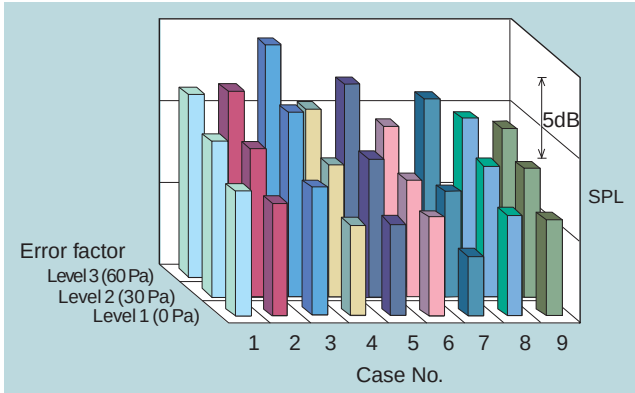

Fig. 19 Predicted BPF noise level based on Lg (3^4)
Indicates the result of numerical experiment based on orthogonal array (L_9).

A parametric study of the shroud casing by using numerical simulation with the prediction technique above was performed, for the optimization of BPF noise reduction. The case selection of parametric study and the optimization technique are based on the Taguchi method.

Table 4 shows the control factor, error factor and each level for the shroud casing items for this study, while **Fig.18** shows an outline of the control factors. Further, error factor was set as an external static pressure of CRFM on the assumption that the flow channel pressure loss changes according to the layout difference around the fan for each vehicle. The experimental plan was made by assigning the control and error factors to **Table 5** L9 (34) orthogonal table for CRFM. The error factors were set as 3 levels for each experiment case number and the unsteady CFD and BPF noises were predicted for a total of 27 cases. The BPF noise was assessed by the sound pressure level at a position 1 m upstream of the fan axis, which is the noise assessment point usually used for CRFM. Moreover, the noise was predicted in all cases at the constant airflow volume of 1 200 m^3/h.

Figure 19 shows the predicted results for the BPF noise in each case. As shown in the figure, the noise gets worse for each case in the order of the error factors level 1 (0 Pa) to Level 3 (60 Pa) because the fan load is increased by adding an external static pressure at a constant airflow volume. The SN ratio for each case was calculated on the basis of SN ratio formula using the above BPF noise prediction values.

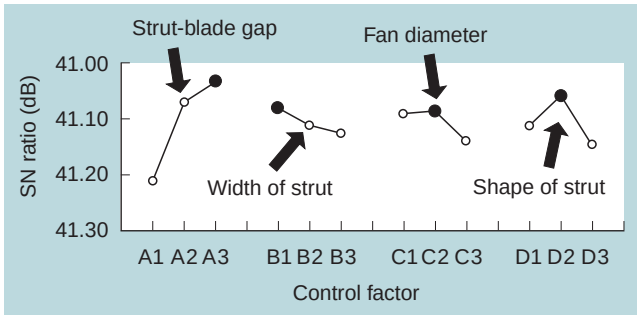

Fig. 20 Control factor effect diagram
Indicates SN ratio of each error factor.

Figure 20 shows the factor effect. The optimum combination of design parameters could be obtained from the present design optimization study, and the SN ratio of each design parameter for BPF noise suggested that the potential interaction of the motor support beam and rotor blade has a dominant influence. These results are useful in the design of shroud casings of automotive CRFMs.

11. Conclusion

A prediction technique using the unsteady CFD results for the BPF noise generated from the CRFM fan has been developed for application to the noise reduction of the automotive CRFMs. A verification test for prediction accuracy was carried out, and it was confirmed, regarding the spatial sound field distribution, that the relative differences of BPF noise can be predicted with an accuracy to less than 1 dB in the regions where solid surfaces causing reflection do not exist between the sound source and the sound reception point. By a minimization study using the Taguchi method on the BPF noise derived from the BPF noise prediction technique, effective data on the CRFM shroud casing was obtained. In the future, this prediction technique will be used in order to accelerate the quantitative study of noise reduction of CRFMs for various vehicles. Moreover, a new analysis code considering reflection and diffraction will be investigated in order to improve the accuracy of the spatial sound field distribution of BPF noise.

References

(1) Curle,N., The Influence of Solid Boundaries upon Aerodynamic Sound, Proc. of the Royal Soc., A231 (1955) p.505

(2) Shiraki, K. et al., Noise Prevention Design and Simulation, Industry and Chemistry Systems (1987)

(3) Kudo, T. et al., Development of Noise Reduction Method for Radiator Fun of Automobile, Japan Society of Mechanical Engineers of Annual Meeting Lecture Collected Papers in 2004 (7) pp.75-76 (2004) (in Japanese)


Atsushi Suzuki


Tetsuo Tominaga


Tsuyoshi Eguchi


Toshifumi Kudo


Tomoshige Takata